THE JOURNAL OF PHYSICAL CHEMISTRY C

Article

Cite This: J. Phys. Chem. C 2019, 123, 16681−16689

pubs.acs.org/JPCC

Influence of Coulombic Interaction on the Interfacial Self-Assembly of Discotic Liquid Crystal Amphiphiles: A Combined Experimental and Computer Simulation Study

Prakhar Verma,[†] Shakkira Erimban,[‡] Nishant Kumar,[†] Snehasis Daschakraborty,*[,‡] Alpana Nayak,*[,†] and Sandeep Kumar[§]

[†]Department of Physics and [‡]Department of Chemistry, Indian Institute of Technology Patna, Patna 801106, India

[§]Raman Research Institute, Sadashivanagar, Bengaluru 560080, India

Supporting Information

ABSTRACT: Self-assembly of amphiphilic molecules largely depends on the structure and electronic properties of the polar head groups. An important class of amphiphiles with technological applications comprises the discotic liquid crystal (DLC) amphiphiles. Here, we report remarkable differences in the self-assembly properties of two similar discotic amphiphiles with dissimilar polar head groups, viz., imidazole-tethered with hexaalkoxytriphenylene (neutral-ImTp) and imidazolium-tethered with hexaalkoxytriphenylene (ionic-ImTp). Surface manometry reveals that the ionic-ImTp exhibits a larger limiting area, higher collapse pressure, and smaller compressional elastic modulus at the air−water interface as compared to the neutral-ImTp system. At the air−solid interface, ionic-ImTp can be transferred only up to a bilayer structure with undulated morphology, whereas the neutral-ImTp exhibits smooth morphology and higher transfer efficiency. These results are explained by density functional theory (DFT) calculations and molecular dynamics (MD) simulations, which elucidated that the Coulombic interaction is the dominant factor that controls the organization of these molecules. DFT calculations predicted a T-shaped π-stacking geometry for the ionic-ImTp and a parallel-displaced stacking geometry for the neutral-ImTp. MD simulation predicted the orientation of molecules and their strength of hydrogen bonding. Understanding the intermolecular interactions governing self-assembly is important to engineer molecular packing that controls the charge transport in DLC-based organic electronics.

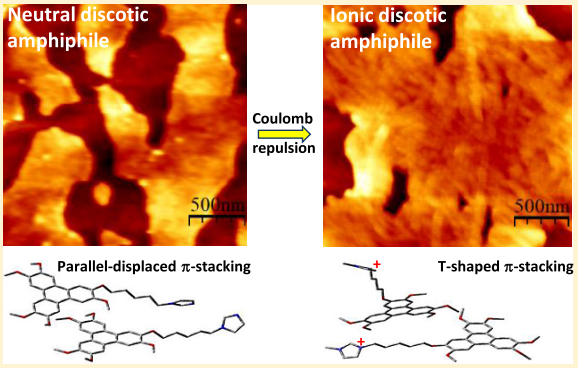

INTRODUCTION

Discotic liquid crystals (DLCs) have emerged as one of the potential components for organic semiconductor devices such as light-emitting diodes, field effect transistors, and solar cells.[1,2] A DLC molecule generally consists of a rigid central core made up of fused aromatic rings and peripheral alkyl chains attached to the core.[3] The anisotropic charge-carrying properties of these molecules are greatly enhanced by the π-stacking interactions between the central aromatic cores.[4] Such interactions are also responsible for self-assembly underlying stable mesophases not only in the bulk but also at interfaces.[5] Unlike bulk, the asymmetric forces at an interface enable distinctly different material properties that shape the dynamic reorganization and response of self-assembled molecules.[6] Nevertheless, interfaces are ideal platforms for the evolution of unique structure/property relations. This provides route to tunable physicochemical architectures for technologically applicable thin films.[7]

Self-assembly is ubiquitous in nature. The fundamental biological process of self-assembly, in which an organized structure builds itself from a collection of smaller units, has been the basis for the creation of all living organisms.[8] This simple process is yet very complex, as evident from the astonishing structures of lipid membranes, folded proteins, and DNA to name a few. Although mimicking such structures is extremely challenging, these have been inspiring researchers to develop nanostructures for applications in emerging nanoscale devices. Interestingly, DLCs with an interlayer spacing of 0.34 nm have been regarded as a chemically synthesized version of DNA-mimic.[9] Moreover, hybrid structures of DLC−DNA complexes have been reported in the bulk[10] as well as at interfaces.[11,12] Currently, the self-assembly properties of DLCs are a hot topic of research because of the unique charge- and energy-transport properties that offer huge possibilities for developing quantum conductive devices.[13]

Among various noncovalent interactions such as van der Waals, entropic, steric, electrostatic, hydrophobic/hydrophilic, and hydrogen bonding, the π-stacking interaction is thought to

Received: March 22, 2019
Revised: May 31, 2019
Published: June 14, 2019

DOI: 10.1021/acs.jpcc.9b02713
J. Phys. Chem. C 2019, 123, 16681−16689

be predominant particularly for the DLC systems.[14] Incorporation of an amphiphilic character by attaching suitable polar head groups offers further tunability of self-assembly properties at interfaces. Moreover, if the polar head group is ionic, the electrostatic interaction starts to compete with other driving forces. Since the π-stacking interaction is known to be dominant among DLCs, any factor that alters the strength of π-stacking between neighboring molecules should have a dramatic impact on their self-assembly properties.

Here, a systematic study of the self-assembly of two similar discotic amphiphiles with dissimilar polar head groups, viz., imidazole-tethered with hexaalkoxytriphenylene (neutral-ImTp) and imidazolium-tethered with hexaalkoxytriphenylene (ionic-ImTp), has been investigated at air−water and air−solid interfaces. While both formed stable monolayers at the air−water interface, there were remarkable differences in the molecular packing and their transfer efficiencies on solid surfaces. These experimental observations are explained by density functional theory (DFT) calculations and molecular dynamic (MD) simulations. It has been revealed that the Coulombic interaction is the dominant factor that gave rise to several interesting aspects such as T-shaped π-stacking geometry, distinct orientations of the molecules, and differences in the strength of hydrogen bonding. It should be mentioned here that a series of experimental studies on similar molecular systems were reported before.[12,15−17] However, computer simulation studies have been carried out, for the first time, on these molecular systems to understand the detailed self-assembly properties. Since thin films of imidazolium-based DLCs have potential for device applications such as solar thermal energy generators and electrolytes for batteries/capacitors,[2] understanding their self-assembly properties is crucial.

METHODS

Experimental Methods. *Materials.* ImTp is a discotic molecule, which consists of a triphenylene core attached to a imidazole (or imidazolium) group by an aliphatic carbon chain as shown in (Figure 1). The imidazole (or imidazolium) part, being hydrophilic in nature, offers a film-forming ability on water surface. These two molecules are similar except for their polar head groups; imidazole is neutral and imidazolium is ionic. The materials neutral-ImTp and ionic-ImTp were synthesized, and their thermotropic liquid crystalline properties were reported earlier.[18] The neutral-ImTp material did not show any liquid crystalline phase in the bulk. On heating, the neutral-ImTp material directly went from a crystalline phase to an isotropic liquid phase at 50 °C. On the other hand, incorporation of an ionic group induced liquid crystal properties. The ionic-ImTp exhibited the following mesophase sequence: solid−columnar, 67 °C; columnar−isotropic, 101 °C. On cooling, the columnar mesophase appeared at 98 °C with the mesophase solidifying at 38 °C.

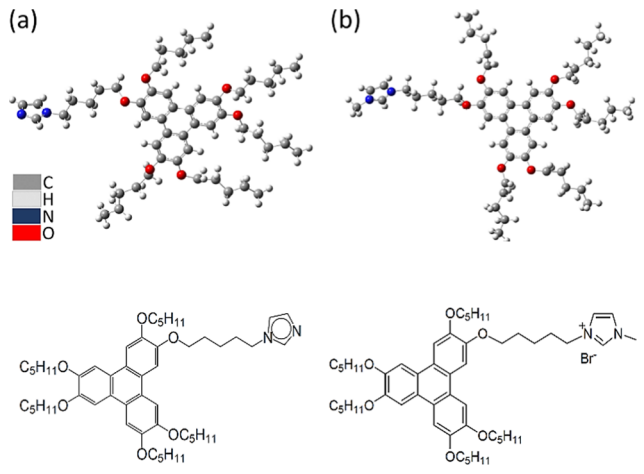

Figure 1. Energy-minimized molecular structures and chemical structures of (a) neutral-ImTp and (b) ionic-ImTp molecules.

Measurements. The surface manometry experiments were carried out using a NIMA 611M Langmuir−Blodgett (LB) trough. The subphase used was ultrapure deionized water (pH 5.8) obtained from a Millipore Milli-Q system. The stock solution of 0.236 mM concentration was prepared using chloroform (HPLC-grade). After spreading the stock solution on the subphase using a Hamilton μL syringe, the film was left for 20 min, allowing the solvent to evaporate. The surface pressure versus area per molecule isotherms were obtained by symmetric compression of the barriers with a constant compression rate of 0.103 nm^2/molecule/min. The surface pressure was measured using the standard Wilhelmy plate technique. The Langmuir−Blodgett (LB) technique was employed to transfer various layers of the films onto hydrophilic and hydrophobic substrates at different target surface pressures with a dipping speed of 2 mm/min. To obtain hydrophilic surfaces, we treated polished silicon wafers for about 5 min with hot piranha solution (mixture of concentrated H_2SO_4 and H_2O_2 in 3:1 ratio), which were then rinsed with ultrapure deionized water and later dried. For hydrophobic surfaces, freshly prepared hydrophilic silicon substrates were dipped in hexamethyldisilazane (HMDS) for 12 h and then rinsed with HPLC-grade chloroform. All films with odd number of layers were transferred onto hydrophilic substrates, and those with even number of layers were transferred onto hydrophobic substrates. The atomic force microscope (AFM) studies on these LB films were performed using a PicoPlus (Molecular Imaging 5500) system. Silicon tips with a spring constant of 21 N/m and resonance frequency of 250 kHz were used. The AFM images were procured using the AC mode in ambient conditions. All of the experiments were carried out at room temperature (~300 K).

Theoretical Methods. *Gas Phase DFT Calculations.* The initial structures of the neutral- and ionic-ImTp molecules were built using Avogadro software.[19] To decrease the computational cost, the carbon chains were reduced to methyl groups only in the DFT calculation. Pairs of neutral- and ionic-ImTp molecules were placed respectively at an interplanar separation of 0.3 nm using Gaussview[20,21] software. The first-principles calculations were carried out for these two systems based on DFT at the B3LYP/6-311G**[22−25] level and basis set. To obtain the energy profile as a function of the interplanar separation between the geometry-optimized structures, single-point energy calculations were performed for each separation between the two molecules.

MD Simulations. MD simulation studies were performed using GROMACS software[26] to obtain a supramolecular assembly of the neutral- and ionic-ImTp molecules in the water−vapor interface. Using packmol software,[27] the initial configuration was built up on the surface of a liquid water slab for four different systems with 25, 34, 50, and 70 molecules of neutral-ImTp and with 25, 37, 73, and 98 molecules of ionic-ImTp (snapshots are shown in the Supporting Information

DOI: 10.1021/acs.jpcc.9b02713
J. Phys. Chem. C 2019, 123, 16681−16689

Figure S1). These numbers were chosen based on the experimental surface area obtained from the isotherm plots (Figure 3). A typical configuration for the system with 70 molecules of neutral-ImTp has been shown in Figure 2. In the

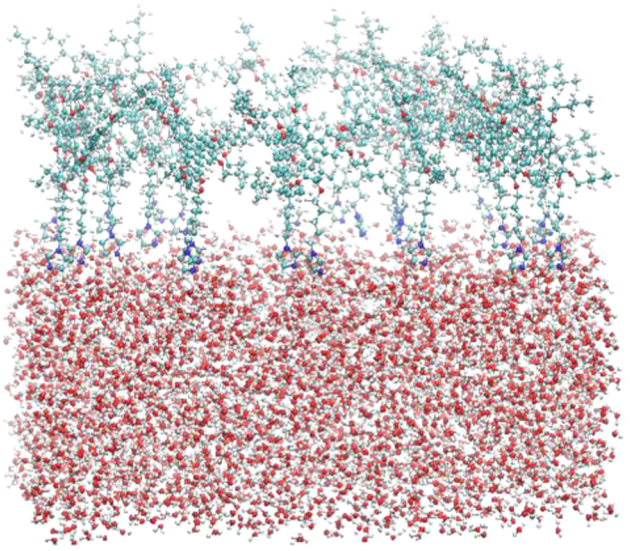

Figure 2. Initial structure of the system generated from Packmol for the surface area of 0.7 nm^2/molecule with 70 neutral-ImTp molecules and 4700 water molecules at 300 K.

case of the ionic system, an equal number of bromide ions were added to maintain the electroneutrality of the system. To create sufficient vacuum along the *Z*-axis, the length of the box was set at 100 Å. Periodic boundary conditions were employed along *X*-, *Y*-, and *Z*-axis. Each simulation trajectory was initiated using a slab of water with thickness ~30 Å (4700 water molecules). The ImTp molecules/ions and the bromide ions were modeled using the OPLS-AA force field.[28−30] The SPC/E force field[31] was chosen for water. All of the systems were first equilibrated at 300 K temperature for 10 ns using an NVT ensemble. All of the bonds were held constraint using the LINCS algorithm.[32] The long-range electrostatic interactions were handled using the particle mesh Ewald summation technique.[33,34] The cutoff radius was set to 0.9 nm. The equilibrated systems were then run for 20 ns during which the configurations were saved every 2 ps. These production trajectories were utilized for various analyses.

In addition, surface pressure (π)−area per molecule (A_m) isotherms were predicted qualitatively using Gromacs.[35,36] The surface pressure is given by $\pi = \gamma_0 - \gamma$, where γ_0 is the surface tension of pure water and γ is the surface tension of water with monolayer. The surface tension γ is given by $\gamma = \frac{1}{2}L_z\left[P_{zz} - \frac{1}{2}(P_{xx} + P_{yy})\right]$, where L_z is the length of the box in the *z*-direction; P_{zz}, P_{xx}, and P_{yy} are the pressure tensor terms; and the fractional term $\frac{1}{2}$ accounts for the presence of two surfaces in the system. A previously reported value[35] of γ_0 of 63 mN/m for the SPC/E water model at 300 K was used in the calculations. Various cutoff values of Lennard-Jones interactions were considered in the calculations.

RESULTS AND DISCUSSION

Experimental Section. The surface pressure (π)−area per molecule (A_m) isotherms of the neutral- and ionic-ImTp molecules on the ultrapure deionized water subphase are shown in Figure 3. The surface pressure is defined as the

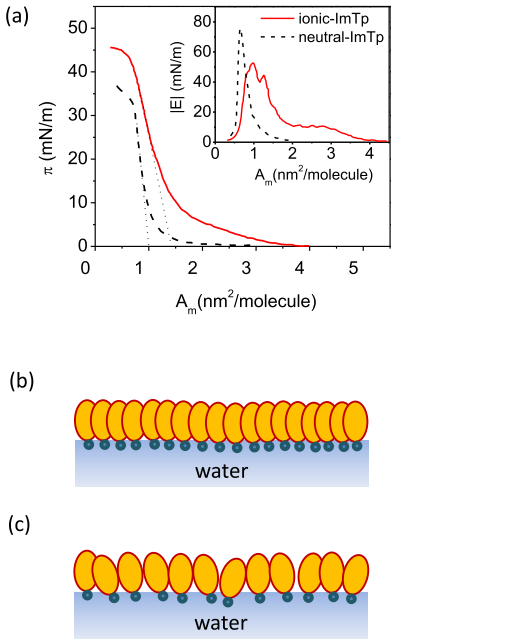

Figure 3. (a) Surface pressure (π) versus area per molecule (A_m) isotherms and compressional elastic modulus (|*E*|) plots for neutral-ImTp (dashed line) and ionic-ImTp (solid line), respectively. (b) Close-packed edge-on arrangement and (c) loosely packed edge-on arrangement of ImTp molecules at the air−water interface.

difference between the surface tensions of water with and without the monolayer. The surface pressure of neutral-ImTp (black dashed line) starts increasing at around an A_m of 2.0 nm^2/molecule, which is followed by a steep rise, until it reaches collapse at ~0.7 nm^2/molecule. The isotherm shows a limiting area (A_o) of 1 nm^2/molecule and a collapse pressure of about 31.4 mN/m. The collapse pressure is defined as the maximum surface pressure that the monolayer can withstand before it collapses and escapes out of the surface in the form of three-dimensional aggregates or crystallites. For the ionic-ImTp isotherm (red solid line), the A_o value and the collapse pressure are significantly high with values of 1.4 nm^2/molecule and 44 mN/m, respectively. The variation of compressional elastic modulus (|*E*|) with A_m for these monolayers is shown in the inset of Figure 3. Here, |*E*| is given by $A_m(d\pi/dA_m)$, which can be calculated from the $\pi-A_m$ isotherms. A maximum |*E*| value of 76 mN/m for the neutral-ImTp monolayer was obtained, which is about 29% higher than the (|*E*|) value attained by the ionic-ImTp monolayer (53.9 mN/m).

On the basis of the molecular dimensions, the obtained A_o values suggest an edge-on arrangement in both the systems. The smaller A_o and larger |*E*| values suggest a close-packed edge-on arrangement in the neutral-ImTp system compared to the loosely packed arrangement in the ionic-ImTp system, as shown in Figure 3b,c. These observations are attributed to the fact that, in the case of an ionic discotic monolayer, there is a competition between two types of interactions: (i) the $\pi-\pi$ stacking interaction between the discotic cores, which favors close packing of molecules in the monolayer, and (ii) the electrostatic repulsion between the molecules, which opposes this close packing.[4]

DOI: 10.1021/acs.jpcc.9b02713
J. Phys. Chem. C 2019, 123, 16681−16689

Next, monolayer films were transferred from the air−water interface to silicon substrates by the LB technique. Figure 4

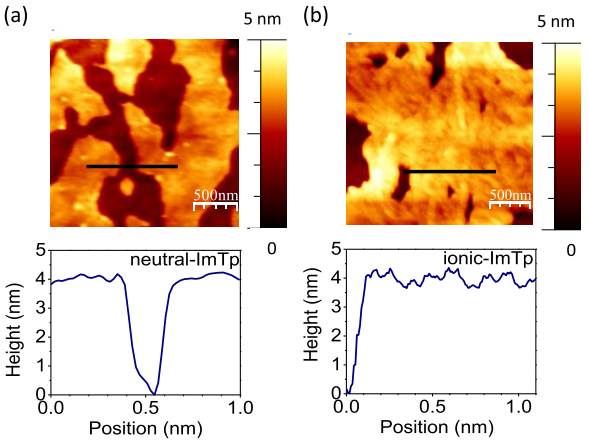

Figure 4. AFM topography images of LB films with two layers of (a) neutral-ImTp and (b) ionic-ImTp on hydrophobic silicon substrates. The respective height profiles corresponding to the lines drawn on the images are shown below. The surface of ionic-ImTp shows undulations (~1 nm), while that of neutral-ImTp is smooth.

shows AFM topography images of LB films with two layers of the neutral-ImTp transferred at 25 mN/m and ionic-ImTp transferred at 35 mN/m onto hydrophobic silicon surfaces. For both the systems, the film height of about 4 nm was obtained, which corresponds to the estimated height of the molecules arranged in an edge-on configuration.[15] Qualitatively, the top surface of the neutral-ImTp film appeared significantly smoother than that of the ionic-ImTp film. The latter showed clear undulations on the surface. The peak-to-peak roughness value was about 1 nm for the ionic-ImTp film and about 0.2 nm for the neutral-ImTp film.

Interestingly, while neutral-ImTp formed multilayers efficiently on silicon surfaces, the ionic-ImTp could not form more than two layers of films. This emphasizes the effect of the ionic polar group on the LB deposition process. To quantify the transfer efficiency, the transfer ratio (τ) was obtained for both the film systems. The τ is defined as the ratio of the decrease in the monolayer surface area to the total surface area of the substrate to be coated. A τ of unity is indicative of perfect deposition. The τ's as a function of number of layers of LB films deposited for the neutral- and ionic-ImTp monolayers are shown in Figure 5 for hydrophilic substrates. It should be mentioned here that, for a hydrophilic substrate, the first downstroke does not coat a monolayer because the hydrophilic surface faces the hydrophobic parts of the amphiphiles. Therefore, the next subsequent upstroke should be considered as the first deposition stroke. The value of τ was close to unity for the first upstroke and the next downstroke of the hydrophilic substrate, leading to the formation of a bilayer structure. However, for the subsequent strokes of film deposition, the τ value was found to decrease. Notably, the efficiency of transfer was observed to be more than 50% even up to 12 layers for the neutral-ImTp system. On the contrary, for the ionic-ImTp system, except for the first two layers, the τ values for the successive cycles of deposition showed desorption in every upstroke and adsorption in every downstroke, thus leading to no net transfer of films.

The dynamics of film deposition can be explained qualitatively based on the complicated physical and chemical

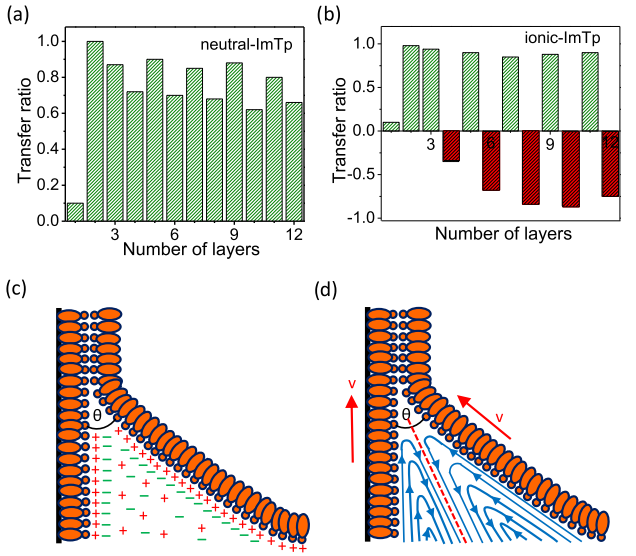

Figure 5. Transfer ratio as a function of number of layers of LB films deposited for (a) neutral-ImTp and (b) ionic-ImTp on hydrophilic silicon substrates. (c) Schematic diagram of diffuse double layer overlapping in the meniscus region during the upstroke deposition of a charged Langmuir monolayer. θ is the dynamic contact angle. (d) Schematic diagram of convective flow in the vicinity of a three-phase contact line. v is the velocity of the surface motion.

processes between the monolayer and substrate. In the literature, it is known that a charged monolayer at the air−water interface and the adjacent diffuse layer of counterions in the subphase form a totally electroneutral electric double layer.[37] The interfacial charge of the ionized surface groups is completely compensated by the opposite charge that is spread out within the diffuse layer. During deposition, close to the three-phase contact line, the electric double layer, which is formed at the air−water interface, overlaps with the double layer at the solid−water interface, as shown in Figure 5c. The overlapping causes deficiency of counterions in the meniscus region.[38] Nevertheless, the deposited LB film from a charged monolayer should be actually electroneutral. Therefore, during the deposition process, the monolayer must bind counterions from the subphase to compensate the surface charge. However, for a complete compensation, all counterions within the diffuse layers should move with the same velocity as the charged surfaces. Generally, the convective flux of the counterions produced by the substrate motion is not sufficient to compensate the flux of the surface charges. This takes place since only those parts of the diffuse layers that are adjacent to the surfaces can move with the same velocity as that of the surfaces in the direction of the contact line, as shown in Figure 5d. The backflow of the subphase expelled from the three-phase contact line hinders the transfer of the counterions to the region of strong overlap of the diffuse layers, thereby hindering the film deposition. Although these explanations are qualitative in nature, they guide us to develop a more quantitative theory, which will be a part of the future work. These are complex dynamics, which are typical of electrodes and membrane systems[39,40] and are also reported for the deposition of arachidic acid monolayer and arachidic salt monolayer under various concentrations of counterions in the subphase.[41,42]

Theoretical Methods. *Gas Phase DFT Calculation.* The geometry-optimized structures obtained from the first-

DOI: 10.1021/acs.jpcc.9b02713
J. Phys. Chem. C 2019, 123, 16681−16689

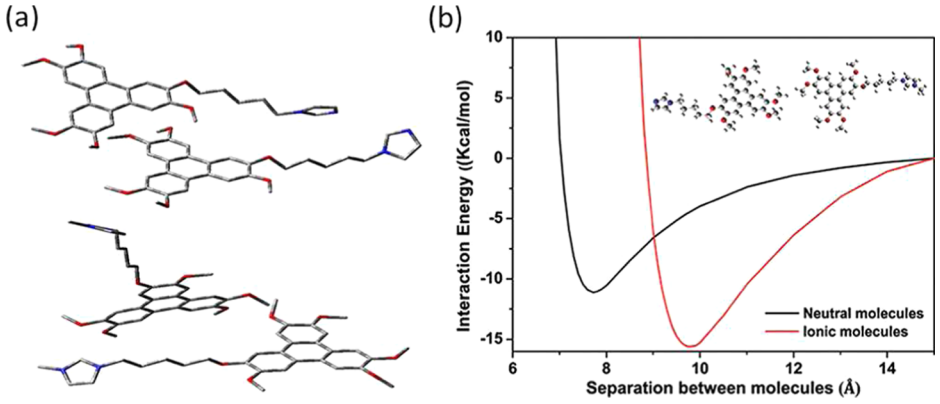

Figure 6. (a) Optimized structures for two interacting neutral-ImTp molecules (top) and ionic-ImTp molecules (bottom) in the gas phase. (b) Interaction energy as a function of separation between the two molecules for neutral- and ionic-ImTp systems.

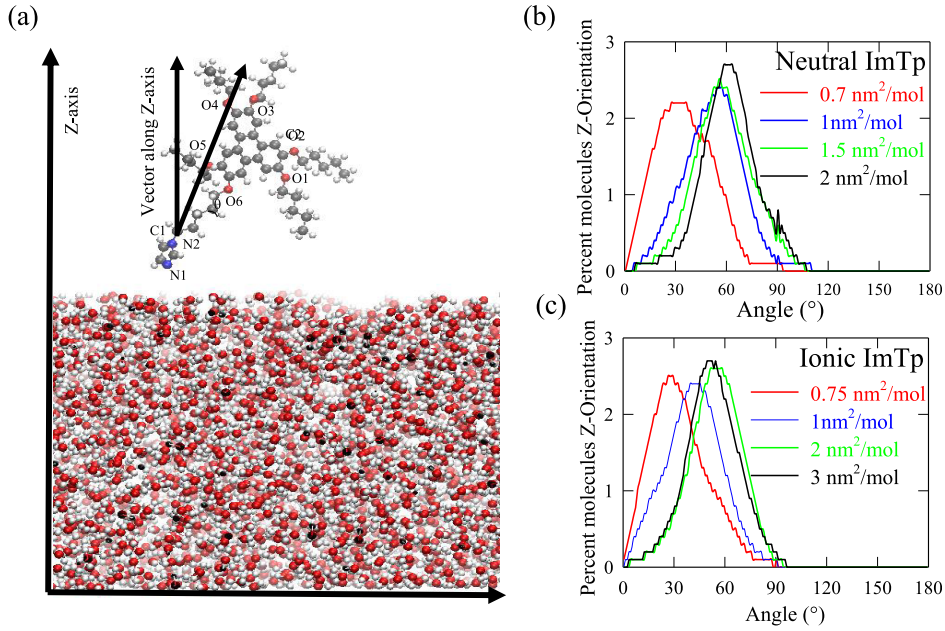

Figure 7. (a) Vector considered for *Z*-orientation along with various labeled atoms. (b) & (c) Percentage of orientation of neutral-ImTp and ionic-ImTp moleculesas a function of the angle with the *Z*-axis for different surface concentrations.

principles DFT calculations showed that π-stacking is a dominant phenomenon among these molecules. The π-stacking of these molecules can be explained by the presence of triphenylene group at the core. While T-shaped stacking geometry was observed for the ionic-ImTp molecules, the neutral-ImTp molecules showed parallel-displaced π-stacking. The optimized structures for both the molecules are shown in Figure 6a. The interplanar separation between the neutral molecules and the ionic molecules are 7.72 and 9.77 Å, respectively, as shown in Figure 6b. The longer interplanar distance between the ImTp ions stems from the electrostatic repulsion between the two imidazolium functional groups. These results are consistent with the experimental observations of larger limiting area per molecule at the air−water interface for the ionic-ImTp as compared to that for the neutral-ImTp (Figure 3). Further, these results explain the differences observed in the morphology of LB films of neutral- and ionic-ImTp systems (Figure 4). While a relatively smooth film surface may stem from the parallel-displaced π-stacking of the neutral-ImTp molecules, the rough and wavy nature of the surface can be a result of T-shaped stacking of the ionic-ImTp molecules. Further details can be obtained by performing simulations on solid surfaces.

Next, the relative stability between the two optimized structures was investigated. The DFT calculation clearly indicated that the T-shaped stacking of ionic-ImTp molecules is more stable than that of the parallel-displaced neutral molecules. Similar stabilization of T-shaped stacking of a benzene dimer is also reported in the literature.[43] Due to the lack of electrostatic repulsion in T-shaped geometry, it has better stability than that of parallel or parallel-displaced stacking. The DFT calculation predicted that the ionic-ImTp molecule is electronically stable by about 4.49 kcal/mol over the neutral-ImTp molecule. The interaction energy as a function of separation between the two ImTp molecules is shown in Figure 6b. This result explains the observation of much higher collapse pressure (~44 mN/m) for the ionic-ImTp monolayer than that for the neutral-ImTp monolayer (~31 mN/m). Notably, the calculation predicted correctly the fact that, despite the stacking of neutral-ImTp molecules being more compact (given by smaller value of A_o), the stability in

DOI: 10.1021/acs.jpcc.9b02713
J. Phys. Chem. C 2019, 123, 16681−16689

the ionic-ImTp system is much higher (given by a higher value of the collapse pressure).

MD Simulations. Orientational Structure. To probe further into the system, the angular distribution of the ImTp molecules on water surface along the vector, as shown in Figure 7a, was obtained. Initial configurations for different concentrations of molecules used for the neutral- and ionic-ImTp systems are shown in Table 1. Lennard-Jones parameters

Table 1. Initial Configuration for Different Concentrations of Molecules Used for the Neutral-ImTp and the Ionic-ImTp Systems As Generated from Packmol for MD Simulations[a]

surface conc.	no. of neutral-ImTp	no. of water molecules
0.7	70	4700
1.0	50	4700
1.5	34	4700
2.0	25	4700
surface conc.	no. of ionic-ImTp	no. of water molecules
0.75	98	4700
1.0	73	4700
2.0	37	4700
3.0	25	4700

[a]Surface concentration is in the unit of nm^2/molecule.

for water and bromide ions used in the simulations are shown in Table 2. The probability densities of the angles between the

Table 2. Lennard-Jones Parameters for Water and Bromide Ions Used in MD Simulations[a]

atom/ion	ϵ (kJ/mol)	σ (nm)
H	0.0000	0.0000
O	0.3166	0.6500
Br	0.4280	2.9706

[a]The cross-parameters are calculated using the Lorentz−Berthelot combination rules.

Z-axis and molecular vector are shown in Figure 7b. For both the systems, as the surface area per molecule decreases, the peak of the angular distribution shifts toward a lower angle. This indicates that the molecules gradually align parallel to the *Z*-axis to attain the edge-on conformation. For the smallest surface area, the molecules become oriented more vertically. However, Figure 7b also shows significant differences in the alignment of molecules in the two systems. For the neutral-ImTp system, while the peak is observed at 60° for the larger surface area of 2.0 nm^2/molecule, the peak shifts to 30° for the smallest surface area of 0.7 nm^2/molecule. However, for the ionic-ImTp system, the peak shifts from 50 to 29° on decreasing the surface area from 3.0 to 0.75 nm^2/molecule. Thus, the surface area influences the alignment of the neutral-ImTp molecules more strongly than that of the ionic-ImTp molecules. In other words, neutral-ImTp molecules exhibit a more closely packed and upright edge-on conformation as compared to the ionic-ImTp molecules. This is consistent with the experimental observation that the surface pressure increases more rapidly for the neutral-ImTp than that for the ionic-ImTp system. Consequently, the compressional elastic modulus of the neutral-ImTp was observed to be ∼29% higher (76 mN/m) than that of the ionic-ImTp monolayer (54 mN/m).

Z-Density of a Head-Group and a Tail-Group Atom. The probability densities of finding a head-group atom and a tail-group atom along the *Z*-axis have been calculated. The nitrogen atoms of the imidazolium group were considered as the head-group atoms and the O6 atom as the tail-group atom. Nitrogen and oxygen atoms are labeled as shown in Figure 7a. The *Z*-density plots for the neutral- and ionic-ImTp molecules are shown in Figure 8a,b, respectively. A major difference

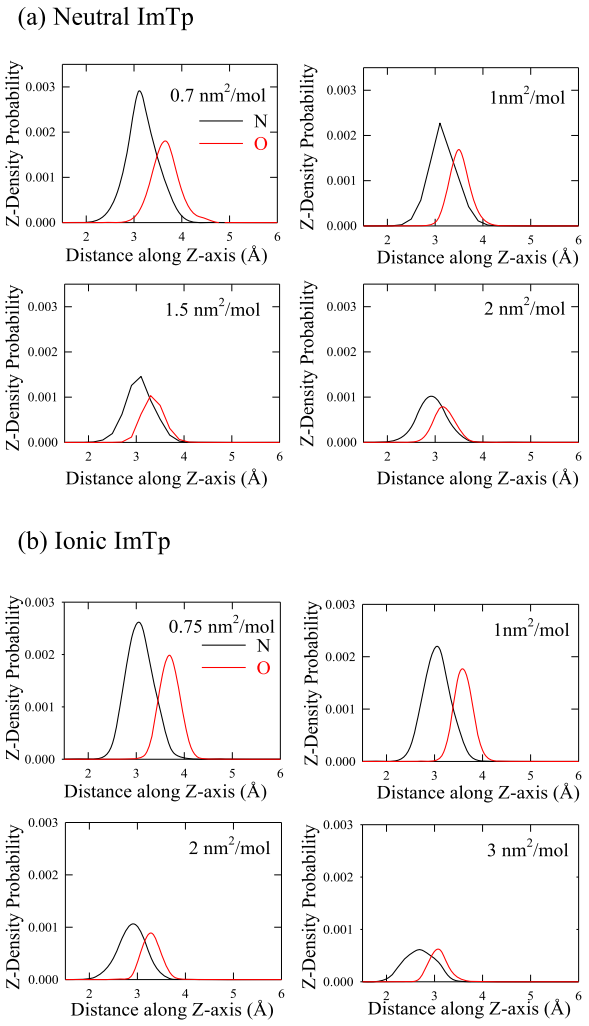

Figure 8. *Z*-Density probabilities for (a) neutral-ImTp and (b) ionic-ImTp molecules as surface concentration varies with respect to the distance along the *Z*-axis.

observed between the two systems is that the separation of the peaks was higher for neutral molecules than for ionic molecules. The higher the separation, the closer the packing of these molecules. This provides further explanation for the experimental results of higher compressional elastic modulus and lower limiting area for the neutral-ImTp as compared to that for the ionic-ImTp molecules.

Hydrogen Bonding. The role of hydrogen-bonding interactions in the stability of films of the neutral and ionic-ImTp molecules at the air−water interface was investigated. The average number of hydrogen bonds between different atoms of the ImTp molecules and water were computed. Here, the widely used geometric definition of the hydrogen bond based on the donor···acceptor heavy atom distance (<3.5 Å) and the donor−hydrogen−acceptor angle (<30°) has been

DOI: 10.1021/acs.jpcc.9b02713
J. Phys. Chem. C 2019, 123, 16681−16689

Table 3. Average Number of Hydrogen Bonds Associated with Different Atoms of Neutral- and Ionic-ImTp Molecules, Obtained from MD Simulations[a]

neutral								
conc.	N1	N2	O1	O2	O3	O4	O5	O6
0.7	1.008	0.492	0.129	0.023	0.010	0.011	0.113	0.206
1.0	1.002	0.531	0.208	0.063	0.054	0.035	0.231	0.312
1.5	1.046	0.549	0.316	0.111	0.071	0.059	0.277	0.371
2.0	1.098	0.596	0.251	0.102	0.103	0.097	0.391	0.432
ionic								
conc.	N1	N2	O1	O2	O3	O4	O5	O6
0.75	0.004	0.003	0.109	0.041	0.006	0.009	0.189	0.206
1.00	0.004	0.003	0.164	0.080	0.007	0.017	0.204	0.210
2.00	0.004	0.003	0.210	0.140	0.045	0.052	0.249	0.233
3.00	0.004	0.003	0.286	0.196	0.022	0.025	0.222	0.219

[a]Surface concentration is in the unit of nm^2/molecule.

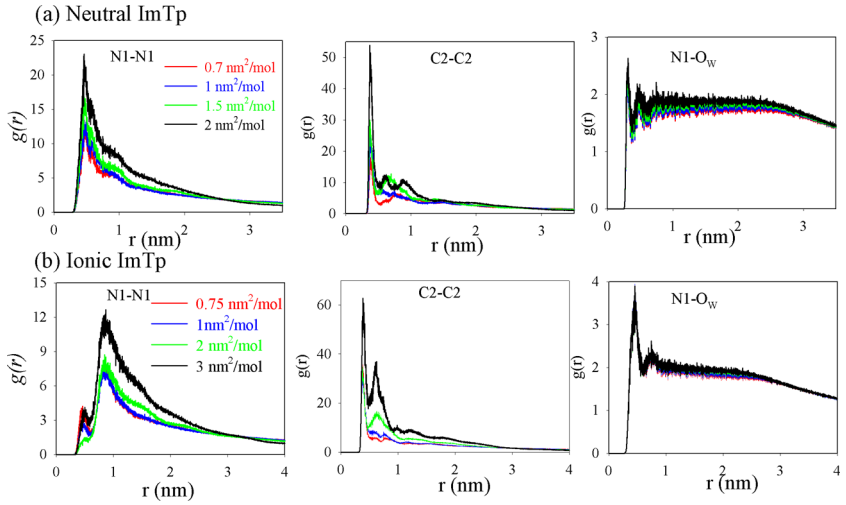

Figure 9. Radial distribution ($g(r)$) as a function of the distance (r) between head-group atoms and water oxygen atoms for (a) neutral and (b) ionic systems.

adopted. The respective numbers of hydrogen bonds for the neutral- and ionic-ImTp molecules are shown in Table 3. For neutral molecules, N1 and N2 atoms actively participated in forming hydrogen bonds with water, whereas for ionic molecules, because of the presence of a positive charge, the hydrogen bonding was rare. Notably, the strength of hydrogen bonding was as high as 2 orders of magnitude for the neutral-ImTp as compared to the ionic-ImTp system. However, hydrogen bonding between the peripheral oxygen atoms and water molecules remained almost the same for both the systems. Further, as the surface area per molecule is decreased, the average number of hydrogen bonds decreases because the molecules tend to orient more toward the Z-axis. Therefore, for smaller surface areas, the distribution of these molecules is more uniform.

Radial Distribution Function. To understand the hydration structure of the head groups and the alignment of head-group atoms among themselves, the radial distribution function $g(r)$ between the head-group atoms and water was calculated. Figure 9 presents $g(r)$'s between N1/C2 atoms of the molecule (see Figure 7 for the atom labels) and water O_w for different surface areas of the neutral and ionic systems. For both the systems, a similar qualitative trend is observed in the $g(r)$ curves. The position of peaks remained the same with varying surface areas. However, the intensities varied. For the $g(r)$ between N1 and N1, the peak intensity was the highest for the system with the maximum surface area per molecule (i.e., 2 nm^2 for the neutral system and 3 nm^2 for the ionic system). This may be due to some sort of structure formation between the molecules. While the first peak arises at about 0.46 nm for the neutral system, for the ionic system, the first peak shifts to around 1 nm. Also, the intensity is higher for the neutral system compared to the ionic system. This indicates a substantial repulsion between the head groups in the ionic system. The first maximum for radial distribution between C2 and C2 is situated at about 0.5 nm for both the neutral and the ionic molecules. The above similarity of the first peak position suggests that the stacking interaction between the fused aromatic regions is unchanged on converting the head group from neutral to ionic. The $g(r)$ curves between the N1 atom and water O_w for the neutral and the ionic systems provide insight into the interaction between the head groups and water. The intensities are observed to be the same for all of the surface areas. This corroborates the fact that the head-group atoms remain strongly hydrogen-bonded with water at the interface. A higher intensity of the first peak is observed for the ionic system compared to that for the neutral system. This is due to the fact that the ionic molecules interact with water much more strongly than the neutral molecules. This is consistent with the H-bond interaction, Table 3.

DOI: 10.1021/acs.jpcc.9b02713
J. Phys. Chem. C 2019, 123, 16681−16689

Further, to investigate the effect of chain length on self-assembly, the simulations were repeated for both the neutral and ionic molecules with reduced carbon chains to methyl groups. The simulation results are presented in the Supporting Information, Figures S2 and S3. Interestingly, the new simulation results are similar and give the same trend of calculated profiles as that obtained for the complete molecules. The only difference is that all of the calculated profiles are much clearer when the simulations are performed with the complete molecules. For instance, in the *Z*-orientational profile (Figure S2), a vertical alignment of the vector with a decrease in surface area per molecule is seen as expected, but a clearer picture can be seen in Figure 7. Similarly, the *Z*-density profiles give a much clearer picture on the vertical alignment of the molecules (as shown in Figure 8) when the simulations were performed for the complete molecule. Therefore, it appears that, unlike fatty acids where alkyl chains are known to be the game changer in determining the phases of monolayer,[44] the self-assembly of discotic molecules are primarily ruled by the discotic core responsible for the π-stacking interaction. Thus, the effect of alkyl chains on the self-assembly of discotic systems seems to be secondary.

Finally, the surface pressure−area isotherms of the neutral and ionic systems were predicted qualitatively (Supporting Information Figure S4). The surface pressure values were calculated for the four different surface concentrations of molecules, as mentioned in Table 1. The calculated values of surface tensions and surface pressures are tabulated in the Supporting Information. As can be seen, although the trend of isotherm can be qualitatively predicted, the calculated values do not match with the experimental ones. Further, the neutral system showed a dip in the isotherm at the point 1 nm^2/molecule followed by an increase as the surface area was reduced. The ionic system showed the expected trend of increasing surface pressure with decreasing surface area. Following the recent report by Javanainen et al.,[36] various cutoff values of Lennard-Jones interactions were used ranging from 0.9 to 2 nm; however, it was found to have a minor influence on the accurate calculation of surface tension. As mentioned by Javanainen et al., most of the simulation models reported so far cannot reproduce experimental pressure−area isotherms with quantitative accuracy. There is a need for proper choice of force-field parameters and an appropriate combination of water models that could provide the correct surface tension for a more realistic MD simulation of Langmuir monolayers. Since the simulation studies of Langmuir monolayers of discotic amphiphiles are not available in the literature, it is a subject of future investigation on how the simulation models for the discotic molecules as well as the combination with different water models influence the simulated isotherm. Thin films of discotic molecules are interesting both scientifically and technologically. The present work predicts the behavior of these molecules at the air−water interface only; however, similar studies at the air−solid interface are in progress.

CONCLUSIONS

Here, the effect of electrostatic interaction on the self-assembly of two similar discotic amphiphiles with dissimilar polar head groups, viz., neutral-ImTp and ionic-ImTp, has been investigated at air−water and air−solid interfaces. While both formed stable monolayers at the air−water interface, the charge on the polar head group played a decisive role in determining the molecular packing and their transfer efficiencies on solid surfaces. The neutral-ImTp formed stable multilayers with as many as 20 layers on silicon surfaces, whereas the ionic-ImTp formed only a bilayer. DFT calculations predicted a T-shaped π-stacking geometry of ionic-ImTp molecules arising due to Coulombic repulsion, which is electronically stable by about 4.49 kcal/mol over the parallel-displaced π-stacking geometry of neutral-ImTp molecules. MD simulations predicted that, due to Coulombic repulsion, the *z*-orientation of the ionic-ImTp molecules changed gradually upon compression as compared to the rapid change observed for the neutral system. Further, comparative analysis of the H-bonding between the neutral and the ionic-ImTp with water molecules revealed a significant reduction of H-bonding strength by about 2 orders of magnitude for the imidazolium group. Finally, a qualitative trend of the isotherms of the neutral and ionic molecules has been predicted based on the simulation results. DLCs are technologically important materials; therefore, understanding intermolecular interactions governing self-assembly is a prerequisite for any successful device application.

ASSOCIATED CONTENT

Supporting Information

The Supporting Information is available free of charge on the ACS Publications website at DOI: 10.1021/acs.jpcc.9b02713.

Calculated values of surface tensions and surface pressures at different surface concentrations; snapshots of the monolayers at 300 K for 0.7, 1.0, 1.5, and 2 nm^2 for the neutral-ImTp molecules and 0.75, 1.0, 2.0, and 3.0 nm^2 for the ionic-ImTp molecules after a 30 ns simulation run; the vector considered for *Z*-orientation along with various labeled atoms for the simplified simulation of systems with carbon chains reduced to methyl groups; the percentage of orientation of ImTp molecules as a function of the angle with the *Z*-axis; for the simplified systems with carbon chains reduced to methyl groups, *Z*-density probabilities as the surface area varies with respect to the distance along the *Z*-axis; and qualitative estimation of the trend of surface pressure−area isotherms of both the neutral and ionic systems (PDF)

AUTHOR INFORMATION

Corresponding Authors

*E-mail: snehasis@iitp.ac.in (S.D.).
*E-mail: anayak@iitp.ac.in (A.N.).

ORCID

Snehasis Daschakraborty: 0000-0002-2694-7142
Alpana Nayak: 0000-0002-3924-0875

Notes

The authors declare no competing financial interest.

ACKNOWLEDGMENTS

Authors thank Dr S. K. Pal at IISER-Mohali for the synthesis of molecules during his Ph.D. under the guidance of Prof. S. Kumar at RRI, Bangalore, India. A.N. thanks the Science and Engineering Research Board, DST, Govt. of India, for the research grant under sanction ECR/2017/002239. Authors thank the reviewers for the constructive suggestions.

DOI: 10.1021/acs.jpcc.9b02713
J. Phys. Chem. C 2019, 123, 16681−16689

REFERENCES

(1) Kato, T.; Yoshio, M.; Ichikawa, T.; Soberats, B.; Ohno, H.; Funahashi, M. Transport of ions and electrons in nanostructured liquid crystals. *Nat. Rev. Mater.* **2017**, *2*, 17001.

(2) Sergeyev, S.; Pisula, W.; Geerts, Y. H. Discotic liquid crystals: a new generation of organic semiconductors. *Chem. Soc. Rev.* **2007**, *36*, 1902−1929.

(3) Chandrasekhar, S.; Ranganath, G. S. Discotic liquid crystals. *Rep. Prog. Phys.* **1990**, *53*, 57−84.

(4) Goossens, K.; Lava, K.; Bielawski, C. W.; Binnemans, K. Ionic liquid crystals: Versatile materials. *Chem. Rev.* **2016**, *116*, 4643−4807.

(5) Kaafarani, B. R. Discotic liquid crystals for opto-electronic applications. *Chem. Mater.* **2011**, *23*, 378−396.

(6) Perova, T. S.; Vij, J. K.; Kocot, A. Observation of an anchoring transition in a discotic liquid crystal. *Europhys. Lett.* **1998**, *44*, 198−204.

(7) Bellier-Castella, L.; Caprion, D.; Ryckaert, J.-P. Surface ordering of diskotic liquid crystals. *J. Chem. Phys.* **2004**, *121*, 4874−4883.

(8) Whitesides, G. M.; Boncheva, M. Beyond molecules: Self-assembly of mesoscopic and macroscopic components. *Proc. Natl. Acad. Sci. U.S.A.* **2002**, *99*, 4769−4774.

(9) *Materials Science of DNA*; Grote, J., Jin, J., Eds.; CRC Press: Taylor and Francis, 2012.

(10) Cui, L.; Miao, J.; Zhu, L. Spacer length controlled oblique-columnar to lamello-columnar mesophase transition in liquid crystalline DNA-discotic cationic lipid complexes. *Macromolecules* **2006**, *39*, 2536−2545.

(11) Mallik, S.; Nayak, A.; Daschakraborty, S.; Kumar, S.; Suresh, K. A. Supramolecular self-assembly of ionic discotic liquid crystalline dimer with DNA at interfaces. *ChemistrySelect* **2018**, *3*, 7318−7326.

(12) Nayak, A.; Suresh, K. A. Discogen-DNA complex films at air-water and air-solid interfaces. *J. Phys. Chem. B* **2008**, *112*, 2930−2936.

(13) Zou, C.; Sun, J.; Wang, M.; Wang, J.; Wu, Y.; Zhang, L.; Zhu, Z.; Xiong, G.; Jiang, L.; Ikeda, T.; Yang, H. A UV-responsive multifunctional photoelectric device based on discotic columnar nanostructures and molecular motors. *Adv. Mater.* **2019**, *31*, No. 1806016.

(14) Foster, E. J.; Jones, R. B.; Lavigueur, C.; Williams, V. E. Structural factors controlling the self-assembly of columnar liquid crystals. *J. Am. Chem. Soc.* **2006**, *128*, 8569−8574.

(15) Nayak, A.; Suresh, K. A.; et al. Films of novel mesogenic molecules at air-water and air-solid interfaces. *J. Phys. Chem. B* **2007**, *111*, 11157−11161.

(16) Nayak, A.; Suresh, K. A. Mechanical properties of Langmuir-Blodgett films of a discogen-DNA complex by atomic force microscopy. *J. Phys. Chem. B* **2009**, *113*, 3669−3675.

(17) Nayak, A.; Suresh, K. A. Conductivity of Langmuir-Blodgett films of a disk-shaped liquid-crystalline molecule−DNAcomplex studied by current-sensing atomic force microscopy. *Phys. Rev. E* **2008**, *78*, No. 021606.

(18) Kumar, S.; Pal, S. K. Synthesis and characterization of novel imidazolium-based ionic discotic liquid crystals with a triphenylene moiety. *Tetrahedron Lett.* **2005**, *46*, 2607−2610.

(19) Hanwell, M. D.; Curtis, D. E.; Lonie, D. C.; Vandermeersch, T.; Zurek, E.; Hutchison, G. R. Avogadro: an advanced semantic chemical editor, visualization, and analysis platform. *J. Cheminf.* **2012**, *4*, 17.

(20) Dennington, R.; Keith, T. A.; Millam, J. M. *Gauss View*, version 6, 2016.

(21) Frisch, M. J.; Trucks, G. W.; Schlegel, H. B.; Scuseria, G. E.; Robb, M. A.; Cheeseman, J. R.; Scalmani, G.; Barone, V.; Petersson, G. A.; Nakatsuji, H. et al. *Gaussian 16*, revision B.01, 2016.

(22) Becke, A. D. Density-functional thermochemistry. III. The role of exact exchange. *J. Chem. Phys.* **1993**, *98*, 5648−5652.

(23) Lee, C.; Yang, W.; Parr, R. G. Development of the Colic-Salvetti correlation-energy formula into a functional of the electron density. *Phys. Rev. B* **1988**, *37*, 785.

(24) Vosko, S. H.; Wilk, L.; Nusair, M. Accurate spin-dependent electron liquid correlation energies for local spin density calculations: a critical analysis. *Can. J. Phys.* **1980**, *58*, 1200−1211.

(25) Stephens, P. J.; Devlin, F. J.; Chabalowski, C. F.; Frisch, M. J. Ab initio calculation of vibrational absorption and circular dichroism spectra using density functional force field. *J. Phys. Chem. B* **1994**, *98*, 11623−11627.

(26) Van Der Spoel, D.; Lindahl, E.; Hess, B.; Groenhof, G.; Mark, A. E.; Berendsen, H. J. C. GROMACS: fast, flexible, and free. *J. Comput. Chem.* **2005**, *26*, 1701−1718.

(27) Martínez, L.; Andrade, R.; Birgin, E. G.; Martínez, J. M. PACKMOL: A package for building initial configurations for molecular dynamics simulations. *J. Comput. Chem.* **2009**, *30*, 2157−2164.

(28) Jorgensen, W. L.; Tirado-Rives, J. Potential energy functions for atomic-level simulations of water and organic and biomolecular systems. *Proc. Natl. Acad. Sci. U.S.A.* **2005**, *102*, 6665−6670.

(29) Dodda, L. S.; Vilseck, J. Z.; Tirado-Rives, J.; Jorgensen, W. L. 1.14*CM1A-LBCC: Localized bond-charge corrected CM1A charges for condensed-phase simulations. *J. Phys. Chem. B* **2017**, *121*, 3864−3870.

(30) Dodda, L. S.; Cabeza de Vaca, I.; Tirado-Rives, J.; Jorgensen, W. L. LigParGen web server: an automatic OPLS-AA parameter generator for organic ligands. *Nucleic Acids Res.* **2017**, *45*, W331−W336.

(31) Mark, P.; Nilsson, L. Structure and dynamics of the TIP3P, SPC, and SPC/E water models at 298 K. *J. Phys. Chem. A* **2001**, *105*, 9954−9960.

(32) Hess, B.; Bekker, H.; Berendsen, H. J.; Fraaije, J. G. LINCS: A linear constraint solver for molecular simulations. *J. Comput. Chem.* **1997**, *18*, 1463−1472.

(33) Darden, T.; York, D.; Pedersen, L. Particle mesh Ewald: An Nlog(N) method for Ewald sums in large systems. *J. Chem. Phys.* **1993**, *98*, 10089−10092.

(34) Essmann, U.; Perera, L.; Berkowitz, M. L.; Darden, T.; Lee, H.; Pedersen, L. G. A smooth particle mesh Ewald method. *J. Chem. Phys.* **1995**, *103*, 8577−8593.

(35) Vega, C.; de Miguel, E. Surface tension of the most popular models of water by using the test-area simulation method. *J. Chem. Phys.* **2007**, *126*, No. 154707.

(36) Javanainen, M.; Lamberg, A.; Cwiklik, L.; Vattulainen, I.; Samuli Ollila, O. H. AtomisticModel for Nearly Quantitative Simulations of Langmuir Monolayers. *Langmuir* **2018**, *34*, 2565−2572.

(37) Kovalchuk, V. I.; Vollhardt, D. Ion redistribution and meniscus stability at Langmuir monolayer deposition. *Adv. Colloid Interface Sci.* **2005**, *114-115*, 267−279.

(38) Kovalchuk, V. I.; Bondarenko, M. P.; Zholkovskiy, E. K.; Vollhardt, D. Influence of ion transfer kinetics on the composition of Langmuir-Blodgett films. *J. Phys. Chem. B* **2008**, *112*, 11333−11340.

(39) Dukhin, S. S. Non-equilibrium electric surface phenomena. *Adv. Colloid Interface Sci.* **1993**, *44*, 1−134.

(40) Lakshminarayanaiah, N. *Transport Phenomena in Membranes*; Academic Press: New York, 1969.

(41) Mahnke, J.; Vollhardt, D.; Stockelhuber, K. W.; Meine, K.; Schulze, H. J. Regular stripe patterns in skeletonized Langmuir-Blodgett films of arachidic acid. *Langmuir* **1999**, *15*, 8220−8224.

(42) Kovalchuk, V. I.; Bondarenko, M. P.; Zholkovskiy, E. K.; Vollhardt, D. Mechanism of meniscus oscillations and stripe pattern formation in Langmuir-Blodgett films. *J. Phys. Chem. B* **2003**, *107*, 3486−3495.

(43) Tauer, T. P.; Sherrill, C. D. Beyond the benzene dimer: an investigation of the additivity of pi-pi interactions. *J. Phys. Chem. A* **2005**, *109*, 10475−10478.

(44) Bell, G. R.; Manning-Benson, S.; Bain, C. D. Effect of chain length on the structure of monolayers of alkyltrimethylammonium-Bromides at the air-water interface. *J. Phys. Chem. B* **1998**, *102*, 218−222.

DOI: 10.1021/acs.jpcc.9b02713
J. Phys. Chem. C 2019, 123, 16681−16689